VOL. 18, NO. 18, SEPTEMBER 2023 ISSN 1819-6608
ARPN Journal of Engineering and Applied Sciences

www.arpnjournals.com

EARLIER DETECTION OF ROP AND ROP SUB-CLASSIFICATION USING TA-CHD-DNN AND UD-TFCM FROM ULTRASOUND DIGITAL B-SCAN IMAGES

K. R. N. Aswini and S. Vijayaraghavan
Department of AIML, KNS Institute of Technology, Bangalore, India
Department of Electronics and Communication Engineering, SCSVMV Deemed University, Kanchipuram, India
Email: krnaswini@gmail.com

ABSTRACT

The growth of the retinal blood vessels of the baby begins at 16 weeks and even after the birth of the baby, they don't grow completely. For the effective analysis of Retinopathy of Prematurity (ROP), diverse methodologies are employed. Owing to the insufficient growth of tangled patterns, greater retinal layer thickness, and the presence of hyperreflective material, the majority of the traditional methodologies were unsuccessful in classifying the Choroidal Neovascularization (CNV), Diabetic Macular Edema (DME), and DRUSEN stages of ROP. Thus, for the classification of different stages of the ROP, an effective Twin Active- Cosine-Hausdorff Distance-Deep Neural Network (TA-CHD-DNN) is proposed in this paper. Chiefly, the image obtained from the retinal image dataset is pre-processed and fed into TA-CHD-DNN. After the extraction of critical features, the segmentation of the retinal layer, choroid layer, and vascular layer occurs in TA-CHD- DNN. The classifier is trained to make decisions for the classification of diverse stages of ROP centered on the extracted features. The normal or abnormal stages of CNV, DME, and DRUSEN are classified by the classifier during testing. By utilizing the Uniformly Distributed-Trapezoidal Fuzzy C Means (UD-TFCM) technique, the decision regarding the severity stage of CNV, DME, and DRUSEN is made in the abnormal stage. Thus, centered on the experimental outcomes, the proposed system performance will be analogized to the conventional techniques to confirm the proposed system's efficiency.

Keywords: retinal blood vessel, segmentation, choroidal neovascularization (CNV), diabetic macular edema (DME), uniform distribution (UD), trapezoidal fuzzy C means (TFCM), twin active- cosine-hausdorff distance- deep neural network (TA-CHD-DNN).

Manuscript Received 23 June 2023; Revised 14 November 2023; Published 30 November 2023

INTRODUCTION

An eye disease that occurs often in infants with low birth weight and premature birth is termed ROP (Hu *et al*., 2019). The disease can either regress spontaneously or progress to a vision-threatening stage as per the natural history of the disease (Rajan *et al*., 2020). Furthermore, globally, every year, approximately 20,000 babies go blind, and 257, 000 years lived with disability globally in 2010 and were associated with visual impairment secondary to ROP as per the estimation of the Global Burden of Disease study (Scruggs *et al*., 2020). Owing to extrafoveal Retinal Detachment (RD), ridge formation with width and height, extraretinal fibrovascular proliferation, subtotal RD encompassing fovea, et cetera, ROP disease majorly emerges (Sun *et al*., 2020). Furthermore, CNV is engendered by the development of damaging blood vessels in the choroid region. The barrier present between the choroid and retina is broken by the CNV and causes blood leakage (vision loss). In addition, even babies suffer from diabetes. Therefore, DME is engendered by the accumulation of excessive fluid in the retina (Chang, 2019). Also, DRUSEN is caused by the presence of smaller yellow or whitish spots in the retina. CNV, DME, and DRUSEN are considered among the diverse retinal diseases owing to their severity in engendering vision blindness in babies. Thus, for the suitable recognition and timely treatment of ROP, multicenter Cryotherapy for ROP and Early Treatment for ROP clinical trials have become important and they can lessen the risk of adverse outcomes along with vision loss (Choi *et al*., 2020).

Inspecting the infants from different views utilizing a digital retinal camera with higher image quality is required for the diagnosis of ROP (Peng *et al*., 2021). After that, to ascertain the presence of ROP's symptoms, experienced ophthalmologists interpreted the imaging data. Nevertheless, as a result of many reasons, namely misidentification owing to the image illumination, eye movement, et cetera, the diagnosis can be challenging. So, as the incidence of disease augments globally, especially in middle-income countries, the demand for ROP screening examinations continues to increase (Redd *et al.,* 2019). Yet, these kinds of screening are expensive for society as well as stressful for infants. Thus, screening routines need to be continuously examined. Preferably, it can also be altered to decrease the number of examinations in infants with a lower risk of treatment-requiring and decrease the expenses of ophthalmological care (Holmström *et al*., 2020). Additionally, regarding the diagnosis of ROP with Artificial Intelligence (AI), numerous studies have accomplished propitious outcomes. The approaches for disease's automated identification in ROP are reliant on conventional approaches, (Tong *et al*., 2020) namely (i) Convolutional Neural Networks (CNN),

(ii) Deep Neural Networks (DNN), (iii) Support Vector Machine (SVM), (iv) Recurrent Neural Networks (RNN), et cetera. However, to offer the accurate classification of the type of ROP like CNV, DME, and DRUSEN, these techniques are still challenging. Certain parameters like retinal thickness and detachment of the retina can be ascertained by utilizing ultrasonic B-scan images. ROP in babies is effectively classified as CNV, DME, and DRUSEN centered on this parameter.

There are still certain limitations that are needed to be solved for better classification even though several machine language and Deep Learning (DL)-based models were created for the classification of ROP type. The following are a few of the limitations of the existing models.

- The percentage of deviation observed in the retina has not been devised as a common parameter. The parameter has to be deemed for an earlier, more effective, and accurate diagnosis of the stage of ROP.
- The ROP prediction has been done manually in previous works. Thus, while formulating classification stages, the position of the B Scan probe should be managed.
- The extraction of optic vascular RD factor and choroidal revascularization from a retinal image has been a challenging task. Hence, it has not yet been deemed for finding the ROP types.

By scrutinizing these downsides, developing an accurate classifier with a reliable clustering technique is the objective of the proposed scheme.

The outline of this paper is arranged as follows: the recent related works of ROP-type classification are elucidated in section 2. The methodologies of the proposed scheme are explicated in section 3. The experimental outcomes of the proposed model are examined in section 4. Lastly, the conclusion and a future suggestion are inferred in section 5.

LITERATURE SURVEY

(Dan *et al*., 2022) constructed a Contrastive Disentangled Network (CDNet) to deal with the Fine-Grained Image Categorization (FGIC) complexities of ocular abnormalities in ultrasound images. (a) Weakly-Supervised Lesion Localization module (WSLL), (b) Contrastive Multi-Zoom (CMZ) strategy, together with (c) Hyperspherical Contrastive Disentangled loss (HCD-Loss) were the '3' necessary components of CDNet. For the ROP severity classification, the experimental outcomes accomplished higher accuracy. Nevertheless, the cross-validation method had a higher computational time.

(Koh *et al.*, 2020) put forward an automated system for detecting RD utilizing texton. The exhibited technique was capable of categorizing the posterior vitreous detachment. When analogized to the prevailing techniques, the constructed technique's outperformance was evinced by the simulation outcomes.

(Chen *et al.*, 2019) created a foveal microvascular structure with ROP. Via cross-sectional Optical Coherence Tomography (OCT) angiography, the foveal thickness was gauged. When pre-processing, the system was still challenged owing to the vanishing problem even though the experimental outcomes displayed a greater accuracy rate.

(Campbell *et al.*, 2021) recommended ROP severity scale employed by clinicians and DL technique. By utilizing a 62 DL algorithm, a quantitative vascular severity score was deployed to every image. The simulation outcomes exhibited that for every formation, the best classifier must be chosen. Nevertheless, on account of utilizing a huge number of data, the system was easily suspected of an overfitting problem.

(Campbell *et al.*, 2017) evinced Handheld OCT Angiography and Ultra-Wide-Field OCT in ROP. By means of a 2nd operator on the computer, the scanning region was controlled. The created system's greater efficacy was displayed by the outcomes. Yet, the system had a greater training time.

(Vural *et al*., 2019) established a technique for the classification of type 1 ROP and Aggressive Posterior ROP (APROP). Only Fluorescein Angiography (FA) was carried out at the baseline. In the experiment, the high classification accuracy exhibited the constructed architecture's efficiency to recognize ROP disease. Nevertheless, the model was unsuccessful in accurately recognizing all of the lesions.

(Silva *et al.*, 2022) revealed an ocular electrophysiology testing along with a videoendoscopic examination to predict visual prognosis in Boston Type 1 Keratoprosthesis (KPro-1) candidate. (i) B-scan ultrasound, (ii) electrophysiological testing, and (iii) Videoendoscopic Evaluation (VE) outcomes were categorized as favourable or unfavourable predictors of postoperative functional outcomes. Therefore, better prognostication in keratoprosthesis candidates was exhibited by the outcomes. Yet, owing to the normally opaque media, prognosis prediction with KPro-I implantation was complex.

(Aswini *et al*., 2020) [26] suggested an Effective, Earlier, along with Simplified Diagnosis of ROP, which was a Probe via a Digital Image Processing (DIP) Algorithm in B-Scan. In this, to gauge the percentage deviation of retinal health concerning prior ultrasonic B scan images, a fresh algorithm was constructed. Therefore, the developed model's higher efficacy was evinced via the experimental outcomes. Yet, when analogized to adults, the fundus was of low contrast in the case of infants and this made the segmentation complex by utilizing the available computer-centered retinal image analyzers.

(Aswini *et al*., 2020) [27] propounded a Probe via the DIP Algorithm in B-Scan. The eye's minuscule

anatomy could be visualized on the monitor inter-phased with the probe by activating.

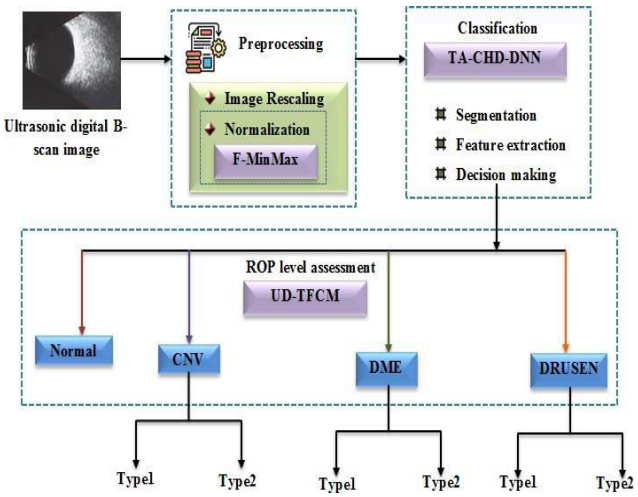

Figure-1. Block diagram of the proposed model.

Preprocessing

At first, from the publically available retinal image dataset, the input training data is amassed. Next, it is wielded for preprocessing. To evade distorted results, Image rescaling and Normalization occur in preprocessing. It is discussed below.

Image Rescaling

In this, to scale retinal features, the incoming high-resolution image I^{hr} is rescaled.

The image with the pixel value of [0, 255] is rescaled. So, the rescaling process $(\Re)$is designed as, the probe at different positions on the closed eyes. The images were occupied with more noise even

$$\Re = I^{hr} \times \chi(3 \cdot \omega) \tag{1}$$

though the created architecture and design would be an effective and accurate diagnosis of RoP in infants.

PROPOSED TA-CHD-DNN-BASED ROP DETECTION AND ROP LEVEL ASSESSMENT METHODOLOGY

One of the most serious health problems in the present world is ROP. For saving the life of infants, ROP's earlier detection is essential. By employing TA-CHD-DNN, an efficient ROP stage classification system is proposed to overcome the complexities available in the existing methodologies in the detection of CNV, DME, and DRUSEN. Figure-1 portrays the proposed

Here, the scaling factor is signified by χ and the height and width of the input image are specified by $\cdot$, ω.

F-MinMax Normalization

In this stage, the rescaled image is normalized. The training process is accelerated by normalizing the rescaled image. The rescaled images are normalized in the range [0, 1] utilizing F-MinMax normalization to guarantee the training outcome's reliability. The rescaled image is indicated as η^{i}. The transformation functions of the F-MinMax normalization is articulated as, classification systems block diagram.

$$\eta^{i} = \frac{\Re - \Re_{\min}}{\max - \Re_{\min}} \tag{2}$$

Where, the initial data is expressed by $\Re$, the maximum and minimum data is signified by $\Re_{\max}$, $\Re_{\min}$, and the normalized data is expressed by η^{i}. So, $(P^{im})$is the output image obtained after preprocessing and it is expressed as, the distance as of the macula to the center of the optic disc. The choroid layer present betwixt the Retinal Pigment Epithelium (RPE) and vascular layer are expressed by Zone 2. The vascular with numerous vascular plexus is articulated by Zone 3. The segmentation of diverse layers is comprehensively

$$P^{im} = \left\{ \Re, \eta^{i} \right\} \tag{3}$$

exhibited below. Centered on the presence of a demarcation line and visible ridge, the retinal layer.

Classification via TA-CHD-DNN

Next, the preprocessed image is fed to the TA-CHD-DNN classifier. A dual function, namely segmentation and decision-making process are carried out by the DNN in the proposed work. So, it is termed a Twin Active (TA). When there is a convex combination at the retinal layer surface distance determined by cross fold, DNN possesses is separated. The Brush annotation technique is wielded for efficient segmentation. It is explicated as follows.

Brush annotation technique: Chiefly, edge-based features are extracted from (P^{im}), and utilizing (4), the corresponding directional histogram (λ) is computed.

A major downside in obtaining rapid conclusions. Hausdorff distance is wielded for gauging the retinal layer surface distance to conquer this issue. Still, the downside of choosing a mismatched point at a long distance prevails. So, it is altered to follow

$$\lambda = \frac{D}{\sum_{i} D} \tag{4}$$

Here, the number of pixels in i^{th} direction is the cosine equation. Furthermore, to offer an effective classification of diverse stages of ROP, the dataset is trained by this algorithm relying on the features extracted utilizing TFCM. Figure-2 evinces the structure of TA-CHD-DNN.

Symbolized by D_i. Afterward, the extraction of the gradient-based features occurs and the corresponding directional histogram is scrutinized. Next, the directional characteristics are represented by drawing a boundary polygon around the demarcation line or ridge (δ). In this, the availability of a whitish line (no blood vessel) betwixt the vascularized and peripheral retina is delineated as the Demarcation line. Further development is undergone by the demarcation line and this engenders the visible ridge. After that, via CHD measurement, the retinal layers (r) are effectively segmented and then labelled accordingly. CHD (C^{hd}) measurement issymbolized as,

$$C^{hd}(\delta, r) = \frac{\sum_{m=1}^{M}\sum_{n=1}^{N} S_{mn}\delta_m r_n}{H(\delta_m r_n)} \quad (5)$$

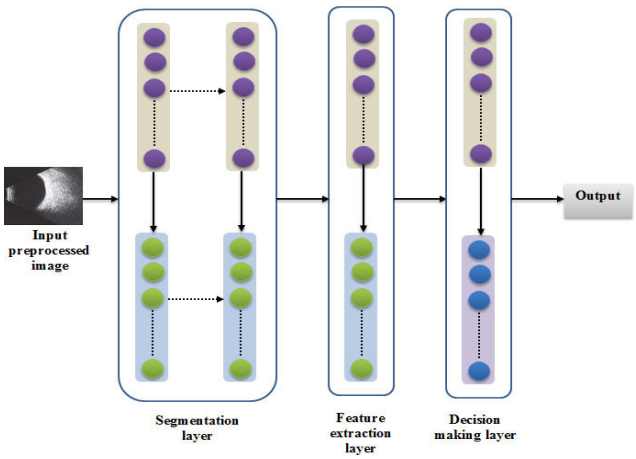

Figure-2. Architecture of TA-CHD-DNN.

The following is the step-by-step process of TA-CHD-DNN.

Where, in (5), the Hausdorff distance between δ and r is explicated by $H(\delta_m, r_n)$, the supremum values are delineated by S and the subset valuesare symbolized by m, n. input layer: Initially, the preprocessed image

$$H(\delta_{m,n}) = MAX(\aleph(\delta_m, r_n), \aleph(r_n, \delta_m)) \quad (6)$$

m n is inputted into the TA-CHD-DNN input m n n m layer and forwarded to the segmentation layer.

Segmentation layer: Next, from the forwarded input, the retinal layer, choroid layer, and vascular layer are segmented. The three-zone concept is utilized for effective analysis. The retinal layer is represented by Zone-1 whose radius is twice the Here, the rank of δ_m depending on r_n is expressed by $\aleph(\delta_m, r_n)$ and the rank of r_n based on δ_m is indicated by $\aleph(r_n, \delta_m)$.

Next, the choroid layer's segmentation occurs. Here, the effective segmentation process is assisted by the presence of irregular patterned choroid vessels. The boundary is made around the choroid vessels and labeled correspondingly by utilizing the brush annotation technique. So, ς refers to the segmented choroid layers. Furthermore, by means of the boundary drawn around the abnormal vascular plexus and labelled, the vascular layer is segmented. Therefore, ϑ expresses the vascular layer. The output of the segmentation layer ($\zeta(i)$) is expounded as,

ROP level assessment

The UD-TFCM technique is espoused to predict the type of ROP severity. For the lower number of clusters, unequal weight factors are assigned in Fuzzy C Means (FCM) clustering. By utilizing a uniform distribution, weights are assigned, and also membership function is then assigned to a trapezoidal fuzzy to conquer this issue. Owing to the modification applied in the general FCM, it is termed UD-TFCM. The UD-

TFCM clustering is explicated below. In this,

$$\zeta(i) = \{r, \varsigma, \vartheta\} \quad (7)$$

extracted features (x_e) are inputted into UD-TFCM.

Feature Extraction layer: From the segmented output, the features are extracted. In this step, the essential features for identifying the disease's y number of cluster centroids (c_k) randomly from x_e. It is articulated as, is selected severity are extracted. Thickness ($thickness'$) and Optical RD risk factors are the features extracted

$$c_k = c1, c2, \ldots\ldots, cy \quad (8)$$

from the retinal layer. Simultaneously, the extraction of certain features, namely vascular severity score and vascular pattern differences, from the vascular layers, takes place, and the

Next, utilizing equation (12), the Euclidean distance ($d\ x_e, c_k$) betwixt the initial pixels x_e and the cluster centroids (c_k) is calculated as, Irregular choroidal (tangled) pattern (Γ) and the beneficiary score regarding the displacement are extracted from the choroid layers.

Therefore, the extracted features (x_e)obtained are expressed as,

$$d(x_e, c_k) = \sum_{k=1}^{y} \left\langle \sum_{k, x_e \in G} \left\| x_e - c_k \right\|^2 \right\rangle \quad (9)$$

$$x_e = \{x_1, x_2, ..., x_E \quad (10)$$

Where, the cluster is expressed by G and $G \geq 1$. Where, the number of extracted features issymbolized by E.

The objective function (ϖ) computed as, of the UD-TFCM is

Decision-making layer: To decide the effective prediction of ROP as normal, CNV, DME, and DRUSEN, the classifier is trained centered on the extracted features. In this, the sigmoid activation

$$\varpi = \sum_{e=1}^{E} \sum_{k=1}^{y} \left(m^{ek}\right)^a \cdot \left[d(x_e, c_k)\right]^2 \quad (11)$$

Where, $_x$the real number greater than 1 is indicated by $1 \leq a \leq \infty$ and it controls the degree of function σe is computed as,

$$\sigma_{x_e} = \frac{1}{1 + e^{-x_e}} \quad (12)$$

fuzziness. The membership function $m^{jk} \in [0, 1]$ is exhibited by m^{jk}.

The trapezoidal fuzzy membership function m^{jk} is

To evaluate the training process, the Mean square error (Ω) is wielded after the effective prediction of ROP. It is assessed below,

$$\Omega = \frac{1}{P} \sum_{p=1}^{\cdot} \left(g_p - t_p\right)^2 \quad (13)$$

Delineated by,

$$m^{jk}(X; v, w, z, Q) = \begin{cases} thickness^r >> 300\mu m; Type2\ DME \\ else; Type1\ DME \\ \rho \leq \gamma \leq \omega, Type1\ DRUSEN \\ \gamma \geq \rho; Type2\ DRUSEN \\ \Gamma, Type1CNV \\ else, Type2\ CNV \\ thickness^r = 300\mu m; \gamma = \Gamma = 0, Normal \end{cases} \quad (14)$$

Here, the desired output is evinced by

g_p and the

$\Gamma, Type1CNV$

actual output for the input features is symbolized

$else, Type2\ CNV$

by t_p . The backpropagation process is not requiredif the error value is equal to the desired output.

Then, the backpropagation process is required for effective analysis in case the error values are not equal to the desired output.

In (14), the trapezoidal membership function in X axis is expressed by $X;v$, w, z, Q. It is transparent that it falls under type 1 DME if the thickness of the retinal layer is greater than $300\mu m$ as of (14). Or else, it engenders type 2 DME. Furthermore, type 1 DRUSEN is engendered by the presence of hyporeflective material (γ) between RPE (ρ) and the junction between the inner and outer segment (ψ) whilst the presence of (γ) greater than (ρ) causes type 2 DRUSEN. Moreover, type 1 CNV is brought about by the presence of tangled patterns (Γ). Type 2 CNV is brought about by the caliber vessel's formation as a branching network. Until the following condition is met, the process is continued by optimizing the objective function (ϖ) by reassigning the cluster centroids c_k and c_i.

Figure-3(a) evinces the input images of the dataset. Figure-3(b) exhibits the Normal Retinal images. Figure-3(c) portrays the DME-affected images. Figure-3(d) depicts the DRUSEN-affected image. Figure-3(e) reveals the CNV-affected image. The types are detected utilizing UD-TFCM after the DME, DRUSEN, and CNV classification. Centered on the retinal layer's thickness, DME types are assessed. Relying on the distance betwixt RPE and the junction betwixt the inner and outer segment, DRUSEN types are assessed. CNV typeis ascertained by the presence of tangled patterns.

Performance Analysis of TA-CHD-DNN

Here, the performance analyses and comparison of proposed TA-CHD-DNN with the prevailing models, namely DNN, Deep CNN

$$\left\| m^{jk}\left(I^t\right) - m^{jk}\left(I^t + 1\right) \right\| \leq \varepsilon \quad (15)$$

(DCNN), and CNN are done.

Where, a constant in the range of 0 to 1 is ε and the number of iterations is specified by I^t. At last, the type of ROP is separated for further identification and analysis centered on the distance and objective function. The following is the pseudocode for the proposed UD-TFCM.

RESULT AND DISCUSSIONS

Here, the proposed model's performance is examined by analogizing its outcomes to other prevailing

models. In the working platform of MATLAB, the proposed model is executed.

Dataset Description

By utilizing the B scan ultrasonic dataset, the experiment is performed in this proposed system. The data has been amassed by conducting some basic eye examination techniques. For training and testing, 83484 images and 968 images are wielded, respectively. Figure-3 portrays the sample input and corresponding output image.

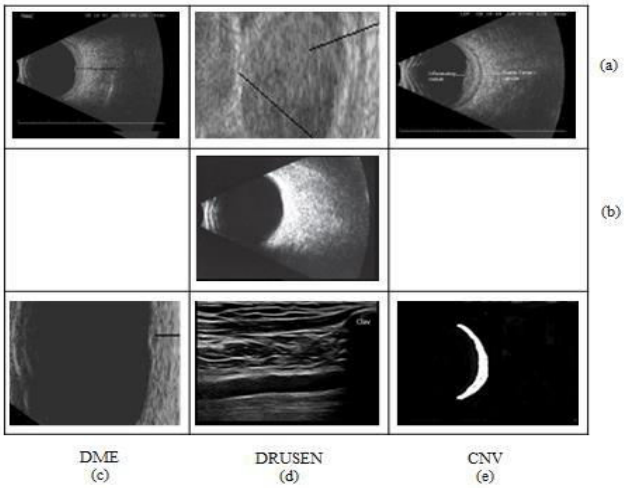

Figure-3. (a) Input images (b) Normal (c) DME (d)DRUSEN (e) CNV.

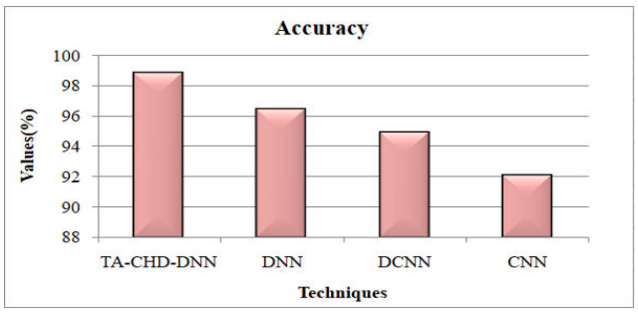

(a)

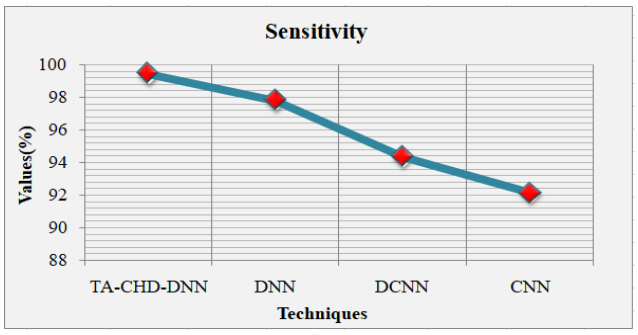

(b)

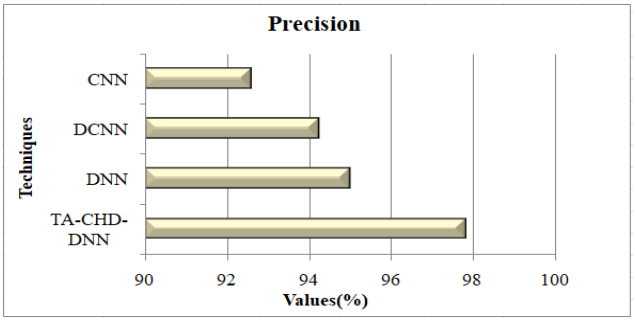

(c)

Figure-4. Comparative analysis of Proposed TA-CHD-DNN and existing models (a) Accuracy (b)sensitivity (c) precision.

Discussion: Regarding accuracy, precision, and sensitivity, the performance of the proposed and traditional methods is exhibited in Figure-4. An accuracy of 98.80% is achieved by the proposed technique. Nevertheless, when analogized to the TA-CHD-DNN technique, the prevailing DNN and DCNN attain lower accuracy of 96.45% and 94.9%, respectively. Similarly, the TA-CHD-DNN methodology has a sensitivity and precision of 99.40% and 97.80%, respectively. Hence, it can be deduced from the overall investigation that the TA-CHD-DNN method exhibits the efficient performance than the prevailing techniques.

Table-1. Performance Analysis of Proposed TA-CHD-DNN and existing models.

Techniques	Youden Index
TA-CHD-DNN	0.97
DNN	0.94
DCNN	0.92
CNN	0.9

Discussion: The performance analysis of the proposed TA-CHD-DNN and prevailing models regarding sensitivity and specificity is displayed in Table-1. The Youden index will denote the performance at a given cut-off if sensitivity, as well as specificity, is diagnostically equally vital or desirable. Therefore, the TA-CHD-DNN method has a Youden index of 0.97, which is 0.03 ameliorated than the prevailing DNN, and 0.07 improved than CNN. The TA-CHD-DNN technique's potency is exhibited.

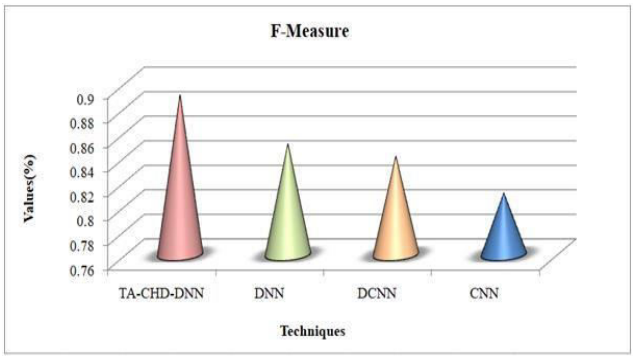

(a)

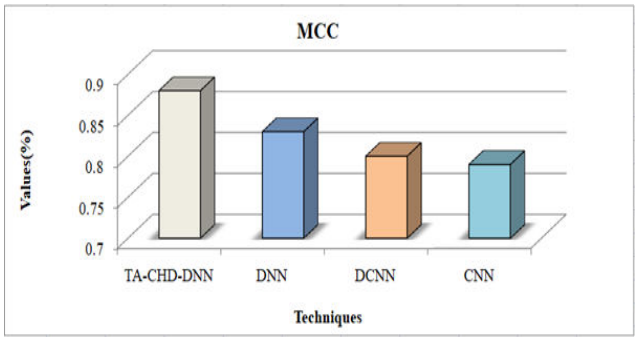

(b)

Figure-5. Comparative analysis of Proposed TA- CHD-DNN and existing models (a) F-measure (b)MCC.

Discussion: The outcomes of the proposed and prevailing techniques are portrayed in Figure-5. For example, The TA-CHD-DNN technique has an F-Measure of 0.89. Nevertheless, the prevailing DNN and DCNN achieved 0.85 and 0.84, respectively. Likewise, the TA-CHD-DNN technique has a Matthews's Correlation Coefficient (MCC) of 0.88 and it is analogized to the prevailing methodologies. Hence, it is inferred from the outcomes of these metrics that the TA-CHD-DNN approach evinces superior performance for the ROP-type classification.

Performance Analysis of UD-TFCM

Regarding the classification rate, the performance of the proposed and traditional techniques, namely FCM Clustering, C Means Clustering (CMC), and K Means Clustering (KMC)is scrutinized and analogized.

Table-2. Performance analysis of proposed andexisting methods.

Techniques	Clustering Accuracy
UD-TFCM	98.70%
FCMC	95.67
CMC	93.22
KMC	921.49

Discussion: The evaluations of proposed and existing techniques are displayed in Table-2. As per this state, the table depicts that the UD-TFCM technique has a classification rate of 98.70%, which is 3.03% enhanced than the prevailing FCMC, and 5.48% enhanced than CMC. It is verified from this comparison that the proposed method is superior to conventional methods.

CONCLUSIONS

ROP-type classification utilizing a novel TA-CHD-DNN classifier is proposed in this work. Pre-processing, classification, feature extraction, and clustering are the processes undergone by the proposed method. Moreover, centered on the presence of tangled (vascular) patterns, retinal layer thickness, and distance betwixt RPE and inner and outer segments of the retina, CNV, DME, and DRUSEN are detected and their types are classified. Regarding various metrics, the experimental analysis is done and the performance of the proposed TA-CHD-DNN was analyzed and analogized to the prevailing methodologies afterexecuting all the steps. An accuracy of 98.80% and a classification rate of 98.70% are achieved by the proposed model, which is exhibited in the final outcomes. Likewise, for all other metrics, namely sensitivity, precision, f-measure, MCC, and Youden index, the best outcome is achieved by the proposed model. Hence, when analogized to theexisting methods, it is deduced from the outcomes of all metrics that the proposed model is highly efficient for the earlier detection of ROP and its types. Yet, this work majorly concentrated on CNV, DME, and DRUSEN. Still, more sub-types in ROP are present, and future works can focus on those sub-types as well as their stages of severity.

Pseudocode for proposed UD-TFCM

Input: Extracted features
Output: ROP level assessed
Begin
Initialize maximum iteration (I^{max})
Calculate cluster centroids (c_k)
For $1 \le k \le y$
Set $I = 1$
Repeat

Determine $d(x_{ek} c_k) = \sum_{k=1}^{y} \left\langle \sum_{k, x_e \in G} \| x_{ek} - c_k \|^2 \right\rangle$
Compute objective function (ϖ)
If (*thickness*^{r} >> 300μm) {
Type2 DME
}Else{
Type1 DME
}End if
If ($\rho \le \gamma \le \psi$){
Type1 DRUSEN
}Else{
Type2 DRUSEN
}End if If$\Gamma = 1$ {
Type1 CNV
}Else{
Type2 CNV
}End ifIf
thickness^r $= 300\mu m; \gamma = \Gamma = 0$ {Normal
}End if
Until $\| m_k(I^t) - m_k(I^t + 1) \| \le \varepsilon$

REFERENCES

Aswini K. R. N., Vijaya R., Sreekanth and Manju S. 2020. Effects of onion extract on hepar histopatology in alloxan-induced diabetic rattus novergicus. Medico-Legal Update, 20(3): 118-122.https://doi.org/10.37506/mlu.v20i3.1451

Aswini K. R. N., Vijaya R., Sreekanth and Manju S. 2020. Effects of onion extract on hepar histopatology in alloxan-induced diabetic rattus novergicus. Nternational Journal of Scientific and Technology Research, 9(3): 5222-5227.https://doi.org/10.37506/mlu.v20i3.1451

Campbell J. P., Kim S. J., Brown J. M., Ostmo S., Chan R. V. P., Kalpathy- Cramer J., Chiang M. F., Jin Kim S., Sonmez K., Schelonka R., Peter Campbell J., Paul Chan R. V., Jonas K., Horowitz J., Coki O., Eccles C. A., Sarna L., Orlin A., Berrocal A., Montero-Mendoza C. 2021. Evaluation of a Deep Learning–Derived Quantitative Retinopathy of Prematurity Severity Scale. Ophthalmology, 128(7): 1070-1076. https://doi.org/10.1016/j.ophtha.2020.10.0 25

Campbell J. P., Nudleman E., Yang J., Tan O., Chan R. V. P., Chiang M. F., Huang D. and Liu G. 2017. Handheld optical coherence tomographyangiography and ultra-wide-field optical coherence tomography in retinopathy of prematurity. JAMA Ophthalmology, 135(9): 977-981. https://doi.org/10.1001/jamaophthalmol.2017.2481

Chang J. W. 2019. Risk factor analysis for the development and progression of retinopathy of prematurity. PLoS ONE, 14(7): 1-9. https://doi.org/10.1371/journal.pone.0219934

Chen Y. C., Chen Y. T. and Chen S. N. 2019. Foveal microvascular anomalieson optical coherence tomography angiography and the correlation withfoveal thickness and visual acuity inretinopathy of prematurity. Graefe's Archive for Clinical and Experimental Ophthalmology, 257(1): 23-30.https://doi.org/10.1007/s00417-018-4162- y

Choi R. Y., Brown J. M., Kalpathy- Cramer J., Chan R. V. P., Ostmo S., Chiang M. F., Campbell J. P., Kim S. J., Sonmez K., Jonas K., Horowitz J., Coki O., Eccles C. A., Sarna L., Orlin A., Berrocal A., Negron C., Denser K., Cumming K., Montero-Mendoza C. 2020. Variability in Plus Disease Identified Using a Deep Learning-Based Retinopathy of Prematurity Severity Scale. Ophthalmology Retina, 4(10): 1016-1021. https://doi.org/10.1016/j.oret.2020.04.022

Dan R., Li Y., Wang Y., Jia G., Ge R., Ye J., Jin Q. and Wang Y. 2022. CDNet: Contrastive Disentangled Network for Fine-Grained Image Categorization of Ocular B-Scan Ultrasound. 1-12. http://arxiv.org/abs/2206.08524

Holmström G., Hellström A., Gränse L., Saric M., Sunnqvist B., Wallin A., Tornqvist K. and Larsson E. 2020. New modifications of Swedish ROP guidelines based on 10-year data from the SWEDROP register. British Journal of Ophthalmology, 104(7): 943-949. https://doi.org/10.1136/bjophthalmol- 2019-314874

Hu J., Chen Y., Zhong J., Ju R. and Yi Z. 2019. Automated analysis forretinopathy of prematurity by deep neural networks. IEEE Transactions on Medical Imaging, 38(1): 269-279. https://doi.org/10.1109/TMI.2018.2863562

Koh J. E. W., Raghavendra U., Gudigar A., Ping O. C., Molinari F., Mishra S., Mathavan S., Raman R. and Acharya U. R. 2020. A novel hybrid approach for automated detection of retinal detachment using ultrasound images. Computers in Biology and Medicine, 120(March): 103704. https://doi.org/10.1016/j.compbiomed.202 0.103704

Peng Y., Zhu W., Chen Z., Wang M., Geng L., Yu K., Zhou Y., Wang T., Xiang D., Chen F. and Chen X. 2021. Automatic Staging for Retinopathy of Prematurity

with Deep Feature Fusion and Ordinal Classification Strategy. IEEETransactions on Medical Imaging, 40(7): 1750-1762. https://doi.org/10.1109/TMI.2021.306575 3

Rajan R. P., Kohli P., Babu N., Dakshayini C., Tandon M. and Ramasamy K. 2020. Treatment of retinopathy of prematurity (ROP) outside International Classification of ROP (ICROP) guidelines. Graefe's Archive for Clinical and Experimental Ophthalmology, 258(6): 1205-1210. https://doi.org/10.1007/s00417-020- 04706-8

Redd T. K., Campbell J. P., Brown J. M., Kim S. J., Ostmo S., Chan R. V. P., Dy J., Erdogmus D., Ioannidis S., Kalpathy-Cramer J. and Chiang M. F. 2019. Evaluation of a deep learning image assessment system for detecting severe retinopathy of prematurity. British Journal of Ophthalmology, 103(5): 580-584. https://doi.org/10.1136/bjophthalmol-2018-313156

Scruggs B. A., Paulchan R. V., Kalpathy- Cramer J., Chiang M. F. and Peter Campbell J. 2020. Artificial intelligence in retinopathy of prematurity diagnosis. Translational Vision Science and Technology. 9(2): 1-10. https://doi.org/10.1167/tvst.9.2.5

Silva L. D., Santos A., Hirai F., Allemann N., Berezovsky A., Salomão R., Oliveira P. R. C. De, Andrade G., Maia A., Sousa L. B. De and De Oliveira L. A. 2022. B-scan ultrasound, visual electrophysiology and perioperative videoendoscopy for predicting functional results in keratoprosthesis candidates. British Journal of Ophthalmology, 106(1): 32-36. https://doi.org/10.1136/bjophthalmol-2020-316962

Sun H., Song J., Kang W., Wang Y., Sun X., Zhou C., Xiong H., Xu F., Li M., Zhang X., Yu Z., Peng X., Li B., Xu Y., Xing S., Wang X. and Zhu C. 2020. Effect of early prophylactic low- dose recombinant human erythropoietin on retinopathy of prematurity in very preterm infants. Journal of Translational Medicine, 18(1): 1-9. https://doi.org/10.1186/s12967-020- 02562-y

Tong Y., Lu W., Deng Q. qin Chen C. & Shen Y. 2020. Automated identification of retinopathy of prematurity by image-based deep learning. Eye and Vision, 7(1): 1-12. ttps://doi.org/10.1186/s40662-020- 00206-2

Vural A., Perente İ., Onur İ. U., Eriş, E., Seymen Z., Hergünsel G. O., Salihoğlu Ö. and Yiğit F. U. 2019. Efficacy of intravitreal aflibercept monotherapy in retinopathy of prematurity evaluated by periodic fluorescence angiography and optical coherence tomography. International Ophthalmology, 39(10): 2161-2169. https://doi.org/10.1007/s10792-018-1040- x